Fluid Dynamics, Vol. 36, No. 1, 2001, pp. 130–138. Translated from Izvestiya Rossiiskoi Academii Nauk, Mekhanika Zhidkosti i Gaza, No. 1, 2001, pp. 145–155.

Three-Dimensional Model of Thermal Convection in an Anisotropic Porous Medium Bounded by Two Horizontal Coaxial Cylinders

O. A. Bessonov and V. A. Brailovskaya

Received June 13, 1999

Abstract — The results of calculating the convective flow in cylindrical porous interlayers are presented as functions of the Rayleigh number, the thickness of the interlayer, and the three-dimensional permeability anisotropy for various methods of specifying the temperature on the cylindrical surfaces. The influence of the three-dimensional effects on the flow structure and heat transfer are analyzed. The existence of single-vortex and multivortex convection regimes is established and the conditions of transition to oscillatory and unsteady flow regimes are investigated in terms of the basic parameters.

The considerable interest [1–11] in the numerical simulation of natural convection in a porous medium bounded by two horizontal coaxial cylinders was initiated by important technological applications. These studies were mainly based on the numerical solution of the two-dimensional Darcy-Boussinesq equations, although for a fairly large ratio of the cylinder length to gap thickness three-dimensional effects develop in the upper half of the annular channel even for low Rayleigh numbers Ra. This was shown in [1], where the critical Rayleigh numbers Ra (as functions of the ratio r_2/r_1 of the radii of the outer and inner cylinders) were obtained. At the critical Rayleigh number the regular two-dimensional convection regimes goes over into unsteady three-dimensional flows.

In [1–7] convection in isotropic cylindrical porous layers was considered. However, porous materials possess considerable permeability anisotropy. In [13] the critical Rayleigh number Ra at which convection develops in an infinite horizontal layer of anisotropic porous material was found on the basis of linearized equations. In [14] convection in plane porous interlayers with allowance for permeability anisotropy was simulated numerically. In [8] the effect of permeability anisotropy on the structure of the flow and heat transfer in annular porous interlayers was investigated and data on the average and local convection characteristics for various Ra numbers and r_2/r_1 were given.

In [5] it was shown that under certain conditions secondary structures exist in the convection flow in an isotropic porous interlayer and the boundaries of these regimes were investigated as functions of the Ra number and the interlayer thickness. The fact that under certain conditions secondary structures develop in homogeneous porous interlayers has been confirmed both experimentally and numerically [7].

In [9], which is a continuation of [2–4, 8], the flow structure in and the heat transfer through porous anisotropic interlayers were simulated numerically within the framework of the two-dimensional model. The development of secondary structures under these conditions also was confirmed. Particular attention was given to the investigation of the effect of permeability anisotropy on the nature of the flow, namely, on the process of restructuring of single- vortex into multivortex flows and vice versa.

In [10] the three-dimensional convection in an isotropic porous cylindrical interlayer was simulated numerically on the basis of a solution of the Darcy-Boussinesq equations in temperature-vector potential variables for the radius ratio $r_2/r_1 = 2$ and an aspect ratio of the length to the radius of the inner cylinder $L/r_1 = 2$ at Ra numbers from 60 to 150. In [11] both two-dimensional and three-dimensional models of the free convection in a cylindrical channel of annular cross-section occupied by an isotropic porous material were investigated.

0015–4628/01/3601–0130$25.00

In the present paper, the convection in a cylindrical anisotropic porous interlayer of large aspect ratio ($L/r_1 = 16$) is simulated numerically in the three-dimensional formulation under conditions of internal heating, i.e., when the temperature of the inner cylinder is higher than that of the outer one. Both steady-state and oscillatory regimes and transitions to unsteady flows are studied for two cylindrical interlayers of different thickness ($r_1/r_2 = 2$ and $\sqrt{2}$) as functions of the Ra number and the relation between the permeability coefficients in the spatial directions.

1. FORMULATION OF THE PROBLEM

In the variables $\mathbf{V}$, p, and T (velocity, pressure, and temperature, respectively), using the linear Darcy's law and the Boussinesq approximation for the lift forces, we can write the equations of free convection in a cylindrical anisotropic porous interlayer in the form:

$$\mathbf{V} = \frac{K}{\mu}(-\nabla p - \rho_0 \mathbf{g}\beta T) \tag{1.1}$$

$$\nabla \cdot \mathbf{V} = 0 \tag{1.2}$$

$$\frac{\partial T}{\partial t} + \rho_0 c_p[\nabla(\mathbf{V}T)] = \lambda^* \nabla^2 T \tag{1.3}$$

$$K = E[k_\varphi, k_z, k_r]^{\mathrm{T}}$$

Here, K is the permeability tensor, E is the unit tensor, ρ_0 is the density of the liquid filling the pores, β is the temperature expansion coefficient, c_p is the specific heat of the liquid, λ^* is the effective thermal conductivity of the porous medium without allowance for convection, μ is the dynamic viscosity, and k_r, k_φ and k_z are the permeabilities of the porous medium in the radial, azimuthal and longitudinal directions, respectively.

We will consider the problem of thermal convection in a cylindrical layer $r_1 r r_2$ of length L on the basis of Eqs. (1.1)–(1.3). In the generic case the boundary conditions have the form:

$$r = r_i, \qquad i = 1,2, \qquad T_i(z) = \langle T_i \rangle + (zL^{-1} - 0.5)\Delta T_i, \qquad V_r = 0$$

$$z = 0, L: \qquad V_z = \frac{\partial T}{\partial z} = 0$$

where ΔT_i are the longitudinal temperature drops on the inner and outer walls ($i = 1,2$).

For investigating the three-dimensional effects we will use four types of boundary conditions for the temperature

$$\Gamma_1: \quad \Delta T_1 = \Delta T_2 = 0, \qquad \langle T_1 \rangle - \langle T_2 \rangle = 1 \tag{1.4}$$

$$\Gamma_2: \quad \Delta T_1 = \Delta T_2 = 0.2, \qquad \langle T_1 \rangle - \langle T_2 \rangle = 1 \tag{1.5}$$

$$\Gamma_3: \quad \Delta T_1 = 0.2, \Delta T_2 = 0, \qquad \langle T_1 \rangle - \langle T_2 \rangle = 1 \tag{1.6}$$

$$\Gamma_4: \quad \Delta T_1 = \Delta T_2 = 0.2, \qquad \langle T_1 \rangle - \langle T_2 \rangle = 0 \tag{1.7}$$

In reducing the system (1.1)–(1.3) to dimensionless form, we take the quantities r_1 (the radius of the inner cylinder), $\lambda^*/(c_p \rho_0 L)$, $\langle T_1 \rangle - \langle T_2 \rangle$, $\lambda^* \mu/(c_p \rho_p k_0)$, and $k_0 = \max(k_\varphi, k_z, k_r)$ as the length, velocity, temperature, pressure, and permeability scales, respectively.

We obtain the following system of equations

$$\mathbf{V} = K(-\nabla p + \mathrm{Ra}^* \mathbf{e}_g T) \tag{1.8}$$

$$\frac{\partial T}{\partial t} + \nabla(\mathbf{V}T) = \nabla^2 T \tag{1.9}$$

$$\mathrm{Ra} = \frac{\rho^2 g \beta (\langle T_1 \rangle - \langle T_2 \rangle) r_1 c_p k_0}{(\mu \lambda^*)}$$

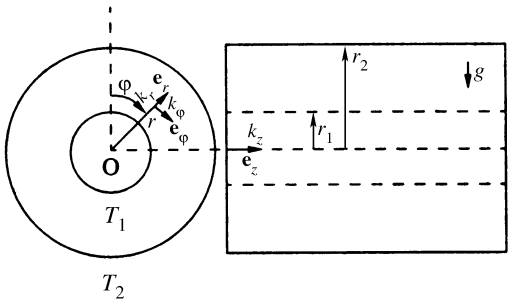

Fig. 1. Channel flow computation diagram.

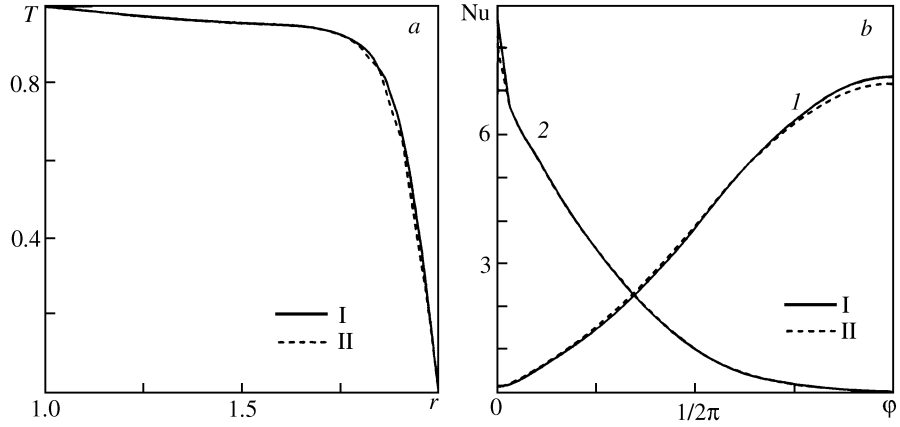

Fig. 2. Profiles of the temperature $T(r)$ (*a*) and the function $\mathrm{Nu}_i(\varphi)$ (*b*) on the inner and outer (curves *1* and *2*) boundaries of the channel in the mid-section $z = 8$ for $\mathrm{Ra} = 200$, boundary conditions Γ_1, variant a (curves I and II correspond to the $64 \times 128 \times 32$ and $64 \times 128 \times 16$ grids, respectively).

Here, Ra is the seepage Rayleigh number, $\mathbf{e}_g = \mathbf{g}/|\mathbf{g}|$ is the unit vector of the gravity force, and $\mathbf{V}$, p, and T are the dimensionless velocity, pressure, and temperature, respectively.

In addition to the characteristics of the flow and the temperature field, we will determine the local and average Nusselt numbers on the inner and outer walls of the region in the middle cross-section $z = L/2$

$$r = r_i, \quad \mathrm{Nu}_i(\varphi) = \frac{\partial T}{\partial r}, \quad \langle \mathrm{Nu}_i \rangle = \frac{1}{2\pi} r_i \int_0^{2\pi} \mathrm{Nu}_i(\varphi)\, d\varphi, \quad i = 1,2 \tag{1.10}$$

As the initial conditions we will take a temperature distribution linear along the radius and a zero velocity field inside the cylindrical channel.

2. METHOD OF SOLUTION

For solving Eqs. (1.8), (1.9) we employed the finite volume method. Uniform spaced grids were used. Second-order central differences were used for discretizing the convective terms in the temperature equation (1.9).

Equations (1.8)–(1.9) were solved separately using the projection method modified for the Darcy-Boussinesq equation.

The calculation algorithm consisted of the following stages: calculation of the intermediate velocity on the basis of the finite-difference analog of Eq. (1.8); solution of the Poisson equation for the pressure and correction of the velocity field; determination of the temperature field using the velocity obtained.

The finite-difference system of temperature equations was integrated in time using the implicit Crank-Nicholson scheme. The Fourier method was used for solving the Poisson equation. This direct method of

solution ensures the high computational efficiency of the algorithm and makes it possible to simulate three-dimensional time-dependent processes numerically on $64 \times 128 \times 32$ grids (in the φ, z, and r directions, respectively). The time taken to compute a single variant of the problem on this grid does not exceed 1 hour for a PentiumPro PC. As distinct from the studies mentioned in the Introduction, the problem is solved over the entire domain without additional assumptions concerning symmetry. The steady-state solutions are symmetric about the vertical diametral plane ($\varphi = 0$) and the violation of symmetry is one the first symptoms of transition to the unsteady flow regime.

The method was tested by comparing the calculations carried out on $64 \times 128 \times 16$ and $64 \times 128 \times 32$ grids. In Figs. 2*a* and 2*b* we have reproduced the calculation results for variant *a*($k_r = k_\varphi = k_z = 1$, boundary conditions Γ_1, and $\mathrm{Ra} = 200$) in the middle cross- section ($z = 8$), namely, the temperature profile $T(r)$ at $\varphi = 0$ and the local Nusselt numbers Nu_1 and Nu_2 on the inner and outer surfaces. For these grids the calculation results (curves *I* and *II*) are fairly similar (the maximum difference is 2.5%). Therefore, in the main calculations we used the more economical $64 \times 128 \times 16$ grid, which also ensured a satisfactory three-dimensional representation of the boundary layers in the neighborhood of $r = r_1$ and $r = r_2$.

3. RESULTS OF THE PARAMETRIC INVESTIGATIONS

Table 1 gives the main results of our parametric investigations in the form of average values of the Nusselt numbers $\langle \mathrm{Nu}_1 \rangle$ on the inner cylindrical surface ($r = r_1$) in the cross-section $z = 8$.

In Table 1 the letters *a–f* denote the variants with various dimensionless permeability coefficient distributions in the directions k_r, k_φ, and k_z and the letters Γ_1, Γ_2, Γ_3, and Γ_4 denote the boundary conditions on the cylindrical surfaces (1.4)–(1.7). For variants with a steady-state flow regime the steady values of $\langle \mathrm{Nu}_1 \rangle$ are given and for variants with periodic oscillations the minimum and maximum values of $\langle \mathrm{Nu}_1 \rangle$. Unsteady regimes with aperiodic (chaotic) oscillations are denoted by "Unst". Thus, Table 1 provides a flow regime map over a wide parameter range.

In order to estimate the three-dimensional effects it is useful to compare the variants with boundary conditions Γ_1 and Γ_2, which have similar parameters. In fact, the latter variant realizes the two- dimensional formulation of the problem since in it there is no horizontal temperature gradient on the cylindrical surfaces and $k_s = 0$ is assumed. The replacement of $k_z = 0$ by $k_z = 1$ in boundary conditions Γ_1 changes neither the flow regime nor its characteristics. The temperature difference ΔT between the cylindrical surfaces initiates a convective flow identical in all annular cross-sections perpendicular to the z axis.

As can be seen from Table 1, for $\mathrm{Ra} = 200$ and 300 ($r_2/r_1 = 2$) and $k_z = 0.2$ the values of $\langle \mathrm{Nu}_1 \rangle$ are almost equal for boundary conditions Γ_1 (variant *b*) and Γ_2 (variants *b* and *c*), and in the three-dimensional formulation for $k_z = 1$ (variant *b* for conditions Γ_2) $\langle \mathrm{Nu}_1 \rangle$ exceeds the corresponding value for Γ_1 by not more than 0.5%, all other permeability coefficients being equal. Thus, for moderate Rayleigh numbers the two-dimensional formulation of this problem is completely justified for calculating engineering heat transfer characteristics.

On the other hand, in the absence of temperature difference ($\Delta T = 0$) between the cylindrical surfaces, when a constant horizontal temperature gradient ($\Delta T_1 = \Delta T_2 = 0.2$ — boundary conditions Γ_4 in Table 2) is maintained, i.e., in the presence of a linear dependence of $T(z)$ on the outer and inner boundaries, convective flows develop. These flows are directed along z toward the right and left in the upper and lower halves of the channel, respectively. This can be seen from the temperature isoline maps in the middle annular and vertical longitudinal sections (Figs. 3*a* and 3*b*). On the inner and outer boundaries of the annular channel in the vertical mid-section of the cylinder the values of the local Nusselt numbers (Fig. 3*c*) are an order of magnitude less than the analogous values of $\mathrm{Nu}_i(\varphi)$ for boundary conditions Γ_2. The behavior of the curves, which are symmetric about zero, gives a zero value of $\langle \mathrm{Nu} \rangle$ (Table 1, the boundary condition Γ_4).

Thus, in the presence of both longitudinal and radial temperature gradients (conditions Γ_2) the three-dimensional convective flow through the porous medium between the cylinders is a superposition of the above- mentioned flows corresponding to boundary conditions Γ_1 and Γ_4.

The boundary conditions Γ_3 are a particular case of conditions Γ_2 for which the outer cylindrical surface

Table 1

Γ_i	N	k_r	k_φ	k_z	$\mathrm{Ra}(r_2/r_1=2)$					$\mathrm{Ra}(r_2/r_1=\sqrt{2})$				
					200	300	500	800	1200	200	300	500	800	1200
Γ_1	*a*	1	1	0	3.846	Unst	–	–	–	4.369	5.369	–	–	–
Γ_1	*a*	1	1	1	3.846	Unst	–	–	–	4.369	5.369	–	–	–
Γ_1	*b*	0.2	1	0	3.549	4.417	–	–	–	–	–	–	–	–
Γ_1	*b*	0.2	1	0	3.549	4.417	–	–	–	–	–	–	–	–
Γ_2	*a*	1	1	1	Unst	Unst	–	–	–	–	–	–	–	–
Γ_2	*a*	1	1	0.2	3.848	Unst	–	–	–	–	–	–	–	–
Γ_2	*b*	0.2	1	1	3.556	4.437	–	–	–	–	–	–	–	–
Γ_2	*c*	0.2	1	0.2	3.551	4.419	5.785	7.350	8.967	–	–	5.355	6.84	–
Γ_2	*d*	0.2	0.6	0.6	2.813	3.493	4.574	5.825	Unst	–	–	4.229	5.31	Un st
Γ_2	*e*	0.2	0.2	1	1.705–2.338	2.022–2.917	–	–	–	2.924	2.812–3.285	–	–	–
Γ_2	*f*	0.2	1	0.6	3.554	4.424	5.792	7.360	8.970	–	–	–	–	–
Γ_3	*a*	1	1	1	Unst	Unst	–	–	–	–	–	–	–	–
Γ_3	*b*	0.2	1	1	3.549	Unst	–	–	–	–	–	–	–	–
Γ_3	*e*	0.2	0.2	1	1.701–2.327	2.021–2.866	–	–	–	–	–	–	–	–

Table 2

Γ_i	N	k_r	k_φ	k_z	$\mathrm{Ra}(r_2/r_1=2)$										$\mathrm{Ra}(r_2/r_1=\sqrt{2})$			
					200		300		500		800		1200		500		800	
					$\langle \mathrm{Nu}_1 \rangle$	V_z	$\langle \mathrm{Nu}_1 \rangle$	V_z	$\langle \mathrm{Nu}_1 \rangle$	V_z	$\langle \mathrm{Nu}_1 \rangle$	V_z	$\langle \mathrm{Nu}_1 \rangle$	V_z	$\langle \mathrm{Nu}_1 \rangle$	V_z	$\langle \mathrm{Nu}_1 \rangle$	V_z
Γ_1	*c*	0.2	1	0.2	3.55	1	4.42	1.49	5.78	2.48	7.35	3.92	8.97	5.82	5.35	1.77	6.84	2.83
Γ_2	*f*	0.2	1	0.6	3.55	2.89	4.24	4.25	5.79	6.84	7.36	10.5	8.97	15.1	–	–	–	–
Γ_2	*d*	0.2	0.6	0.6	2.81	2.85	3.49	4.16	4.57	6.63	5.82	10.1	Unst	–	4.23	5.25	5.31	8.32
Γ_4	*d*	0.2	0.6	0.6	–	–	–	–	–	–	0	11.8	–	–	–	–	–	–

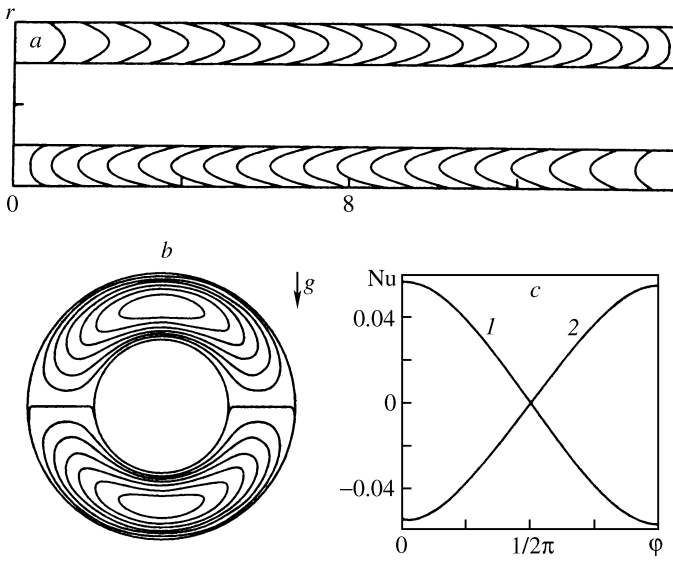

Fig. 3. Isolines of the temperature (*a*) and (*b*) in the longitudinal section $\varphi = 0$ and the cross-section $z = 8$, and the function $\mathrm{Nu}_i(\varphi)$ (*c*) on the inner and outer (curves *1* and *2*) boundaries of the channel in the cross-section $z = 8$ for $\mathrm{Ra} = 800$ and boundary conditions Γ_4, variant *d*.

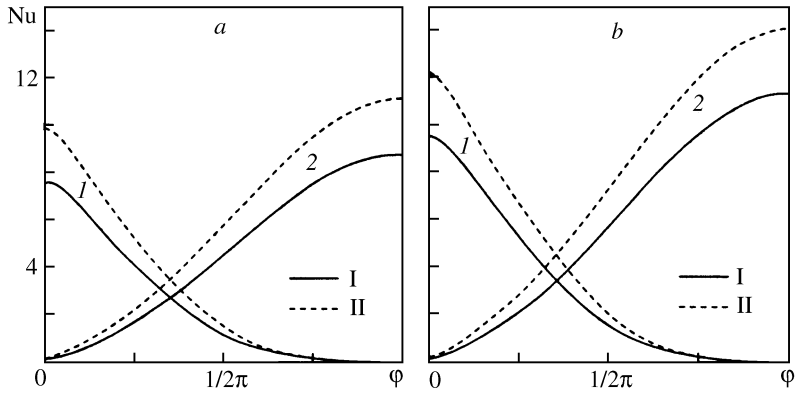

Fig. 4. Dependence $\mathrm{Nu}_i(\varphi)$ (*a*) and (*b*) for variants *d* and *c* on the inner and outer (curves *1* and *2*) boundaries of the channel in the cross-section $z = 8$ for $\mathrm{Ra} = 500$ (I) and $Ra = 800$ (II), and boundary conditions Γ_2.

is isothermal (1.7). In Table 1 we have given the maximum and minimum values of $\langle \mathrm{Nu}_1 \rangle$ for periodic oscillations under conditions Γ_2 and Γ_3. There are no significant differences in either the qualitative (both regimes, periodic and unsteady, are conserved) or quantitative aspects. In variants Γ_2 and Γ_3 in both the steady-state ($\mathrm{Ra} = 200$, variant*b*) and periodic (variant *e*) regimes the maximum difference in $\langle \mathrm{Nu}_1 \rangle$ is less than 2%. Therefore, in what follows, we will mainly consider regime Γ_2.

In Table 2 we have given $\langle \mathrm{Nu}_1 \rangle$ together with the maximum horizontal velocities V_z in the mid-section $z = 8$ for several calculation variants. Variants *c* and *f* could correspond to a textile winding of porous material with azimuthal orientation of the fibers used as insulation and variant *d* to alternating azimuthal and longitudinal orientations.

With increase in Ra the average Nusselt numbers and $|V_z|_{\max}$ also increase in all the variants (*c*, *d*, and *f*), and for narrower interlayers with $r_2/r_1 = \sqrt{2}$ the mean heat flux on the cylindrical surface is always less than that for $r_2/r_1 = 2$.

A comparison of variants c, d, and f makes it possible to estimate the role of the permeability coefficient distribution in different directions. With increase in k_φ, all other things being equal (variants *d* and *f*), $\langle \mathrm{Nu}_1 \rangle$ also increases since the flow with respect to the angular coordinate and the heat transfer become more

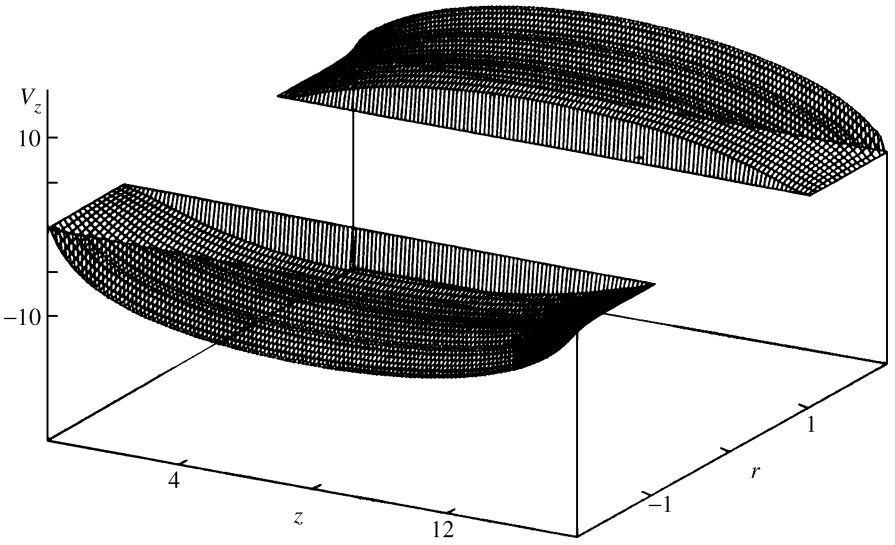

Fig. 5. Velocity fields $V_z(z,r)$ along z in the upper and lower halves of the channel in the longitudinal section for Ra = 800 and boundary conditions Γ_2, variant *d*.

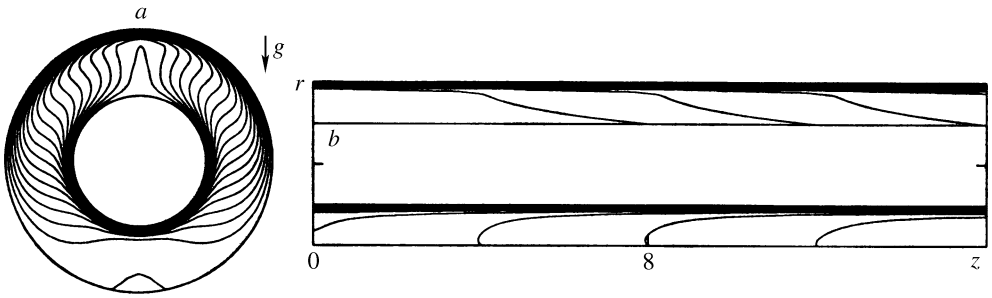

Fig. 6. Isolines of the temperature (*a*) and (*b*) in the cross-section $z = 8$ and the longitudinal section $\gamma = 0$ for Ra = 800 and boundary conditions Γ_2, variant *d*.

intense while the velocity V_z increases only slightly. It is interesting to note that for Ra = 1200 transition to the unsteady regime occurs at a lower azimuthal permeability coefficient $k_\varphi = 0.6$ (variant *d*) as compared with $k_\varphi = 1$ (variant *f*) when the more intense flows and heat transfer in the cross-section stabilize the total convective flow in the volume considered. At the same time, the permeability k_z mainly affects the velocity V_z and the flow stability. In particular, an increase in k_z from 0.2 (variant *c*) to 0.6 (variant *f*) leads to the maximum horizontal velocity V_z increasing by almost threefold, i.e., almost linearly, the corresponding maximum values of $\langle \mathrm{Nu}_1 \rangle$ not being affected.

Thus, the permeability anisotropy leads not only to quantitative changes in the convection intensity (expressed here in terms of $\langle \mathrm{Nu}_1 \rangle$) but also, which is more significant, to qualitative changes, namely, to a change in regimes. In particular, whereas for Ra = 200 (boundary conditions Γ_2) in isotropic interlayers (variant *a*) for $k_z = 1$ an unsteady convection regime in which only instantaneous values of $\langle \mathrm{Nu}_1 \rangle$ can be observed is realized, a decrease in k_z to 0.2 leads to a steady-state regime.

It is also interesting to note the possibility of controlling the flow regime using the permeability parameter in the radial direction. As compared with $k_r = 1$ (variant *a*), a decrease in k_r to 0.2 (variant *b*) leads to weakening of the B*é*nard-type convection in the upper half of the channel and the establishment of a steady-state flow and heat transfer regime. For variants *c*, *d*, and *f* ($k_r = 0.2$) a steady regime is also established up to Ra = 1000 and 1200 (variants *d* and *c*).

For the same value of $k_r = 0.2$ in variant *e* when $k_\varphi = 0.2$ and $k_z = 1$ (as distinct from variant *c* in which, on the contrary, $k_\varphi = 1$ and $k_z = 0.2$), a periodic regime is established so that $\langle \mathrm{Nu}_1 \rangle$ oscillates in

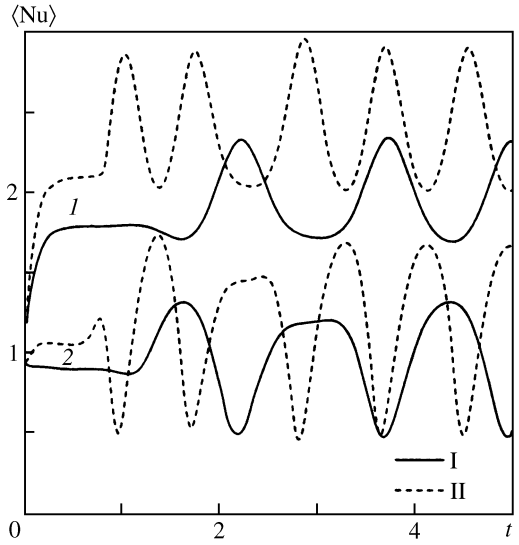

Fig. 7. Dependence $\langle \mathrm{Nu}(t) \rangle$ on the inner and outer (curves *1*and *2*) boundaries of the channel in the cross-section $z = 8$ for $\mathrm{Ra} = 200$ (I) and $\mathrm{Ra} = 300$ (II), and boundary conditions Γ_2, variant *e*.

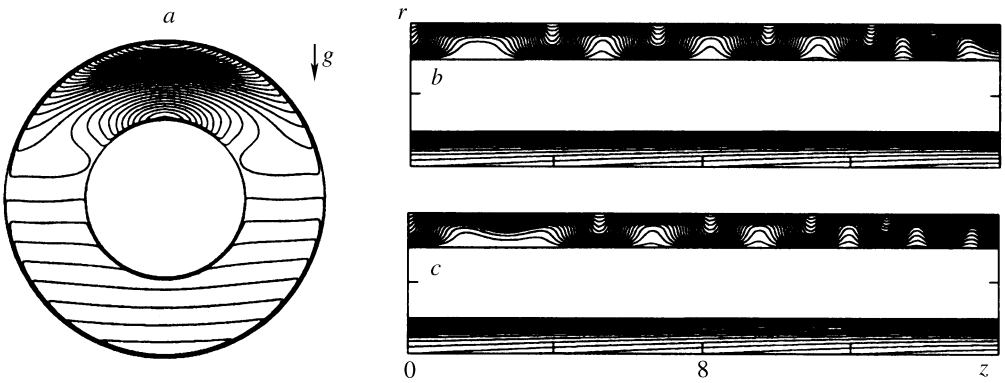

Fig. 8. Isolines of V_z (*a*) in the cross-section $z = 8$ and of the temperature (*b*) in the longitudinal section $\varphi = 0$ for two instants of time, $\mathrm{Ra} = 200$ and conditions Γ_2, variant *e*.

the neighborhood of average values (equal to 2.02 and 2.47 for $\mathrm{Ra} = 200$ and 300) which are smaller than those for variants *c* and *d* since the heat transfer intensity is mainly determined by the permeability in the azimuthal direction.

In addition to considering the average characteristics, it is of some interest to analyze the local characteristics of the flow and heat transfer. In Fig. 4 we have compared graphs of the variation of the local Nu_i numbers on the inner and outer cylindrical surfaces ($i = 1, 2$) for $\mathrm{Ra} = 500$ and $\mathrm{Ra} = 800$ (curves *I* and *II*) for two cases of the permeability coefficient distribution (Figs. 4*a* and 4*b* correspond to variants *c* and *d*). In variant *c* ($k_\varphi = 1$) for both values of Ra the local Nu_i numbers are greater than those in variant *d* ($k_\varphi = 0.6$) over the entire domain of variation of φ. Regardless of k_z, the nonuniformity of the distribution of $\mathrm{Nu}_i(\varphi)$ also increases with k_φ.

An increase in the permeability along z leads to an increase in the velocity V_z (Table 2)., i.e., to a strengthening of the longitudinal horizontal component of the spiral flow in the gap between the cylinders. In Fig. 5 we have schematically plotted a graph of the velocity V_z distribution along z for variant *d* and $\mathrm{Ra} = 800$ as a function of two variables: $V_z(z, r)$. In Fig. 6 we have reproduced the temperature isolines in the mid-section $z = 8$ and the vertical longitudinal section $\varphi = 0$, respectively.

Even for smaller numbers $\mathrm{Ra} = 200$ and $\mathrm{Ra} = 3000$, with increase in k_z an oscillatory flow develops with the formation of secondary vortices along z in the upper half of the cylindrical layer in the same way as

the Taylor-Görtler vortices in the problem of fluid flow in a cavity initiated by the motion of the boundaries [12]. In Fig. 7 we have plotted graphs of the oscillations of $\langle \mathrm{Nu}_i(t) \rangle, i = 1,2$ as functions of time for this case (curves *I* and *II* for Ra = 200 and 300, respectively). Consequently, with increase in Ra the process of approach to a periodic regime is accelerated and the oscillation frequency increases.

The velocity V_z isolines in the cross-section $z = 8$ and the temperature isolines in the vertical longitudinal section $\varphi = 0$ given for two instants of time ($t = 4.4$ and 10) in Figs. 8*a* and 8*b* show that the oscillatory fluid flow through a porous medium filling the upper half of a cylindrical channel leads to a periodic variation of the temperature in this zone. Moreover, this flow affects the velocity V_z distribution in the upper half of the annular cross-section (in Fig. 8*a*) and disturbs the equidistant stratified isoline structure characteristic of the lower part.

Summary. The flow structures, the temperature and velocity fields, and the average and local heat transfer characteristics in the space between horizontal coaxial cylinders filled with an anisotropic porous material is investigated numerically. Three characteristic flow regimes, namely, steady-state, oscillatory, and unsteady (the last goes over into the chaotic regime), are observed depending on the basic parameters: the Rayleigh number, the interlayer thickness, and the three-dimensional permeability coefficient distribution. The role of these factors in the formation of the three-dimensional flow and their relative effect on the restructuring of the flow and heat transfer regimes are demonstrated.

The work was carried out with support from the Russian Foundation for Basic Research (project No. 96-01- 000584).

REFERENCES

1. J.-P. Caltagirone, "Thermoconvective instabilities in a porous medium bounded by two concentric horizontal cylinders," *J. Fluid Mech.*, **76**, 337 (1976).
2. V. A. Brailovskaya, G. B. Petrazhitskii, and V. I. Polezhaev, "Natural convection and heat transfer in porous interlayers between horizontal coaxial cylinders," *Zh. Prikl. Mekh. Tekh. Fiz.*, No. 6, 90 (1978).
3. V. A. Brailovskaya, G. B. Petrazhitskii, and V. I. Polezhaev, "Natural thermoconvection flows in annular porous interlayers," in: *Heat Transfer-1978. Soviet Research* [in Russian], Nauka, Moscow (1980), p. 174.
4. V. A. Brailovskaya, G. B. Petrazhitsky, and V. I. Polezhaev, "Natural thermoconvectional filtration in circular porous interlayers," in: *6th Intern. Heat Transfer Conf. Canada*, Vol. 2 Ottava (1978), p. 239.
5. K. Himasekhar and H. H. Bau, "Two dimensional bifurcation phenomena in thermal convection in horizontal, concentric annuli containing saturated porous media," *J. Fluid Mech.*, **187**, 267 (1988).
6. Y. F. Rao, K. Fukuda, and S. Hasegawa, "Steady and transient analyses of natural convection in horizontal porous annulus with Galerkin method," *Trans. ASME, J. Heat Transfer*, **109**, 919 (1987).
7. M. C. Charrier-Mojtabi, A. Mojtabi, M. Azaiez, and G. Labrosse, "Numerical and experimental study of multicellular free convection flow in an annular porous layer," *Intern. J. Heat and Mass Transfer*, **34**, 3061 (1991).
8. V. A. Brailovskaya, B. P. Kogan, and V. I. Polezhaev, "Effect of permeability anisotropy on convection and heat transfer in a porous annular interlayer," *Izv. Akad. Nauk SSSR, Mekh. Zhidk. Gaza*, No. 1, 59 (1980).
9. V. A. Brailovskaya and L. V. Feoktistov, "Flow structures and heat transfer in anisotropic annular porous interlayers," *Izv. Ros. Akad. Nauk SSSR, Mekh. Zhidk. Gaza*, No. 4, 122 (1998).
10. Y. F. Rao, K. Fukuda, and S. Hasegawa, "A numerical study of three-dimensional natural convection in a horizontal porous annulus with Galerkin method," *Intern. J. Heat and Mass Transfer*, **31**, 695 (1988).
11. M. C. Charrier-Mojtabi, "Numerical simulation of two- and three-dimensional free convection flows in a horizontal porous annulus using a pressure and temperature formulation," *Intern. J. Heat and Mass Transfer*, **40**, 1521 (1997).
12. O. A. Bessonov, V. A. Brailovskaya and B. Roux, "Numerical modeling of three-dimensional shear flow in a cavity with moving lids," *Izv. Ros. Akad. Nauk SSSR, Mekh. Zhidk. Gaza*, No. 3, 41 (1998).
13. G. Castinel and M. Combarnous, "Critere d'apparution de la convection naturelle dans une couche poreuse anisotrope horizontale," *C. Roy. Acad. Sci., Ser. B*, **278**, 701 (1974).
14. T. Nilsen and L. Storesletten, "An analytical study on natural convection in isotropic and anisotropic porous channels," *Trans. ASME, J. Heat Transfer*, **112**, 396 (1990).